2020 IEEE/RSJ International Conference on Intelligent Robots and Systems (IROS)
October 25-29, 2020, Las Vegas, NV, USA (Virtual)

Demonstration of a Novel Phase Lag Controlled Roll Rotation Mechanism using a Two-DOF Soft Swimming Robot

Bangyuan Liu and Frank L. Hammond III, *IEEE Member*

***Abstract*— Underwater roll rotation is a basic but essential maneuver that allows many biological swimmers to achieve high maneuverability and complex locomotion patterns. In particular, sea mammals (e.g., sea otter) with flexible vertebra structures have a unique mechanism to efficiently achieve roll rotation, not propelled mainly by inter-digital webbing or fin, but by bending and twisting their body.**

In this work, we attempt to implement and effectively control the roll rotation by mimicking this kind of efficient biomorphic roll mechanism on our two degrees of freedom (DOF) soft modular swimming robot. The robot also allows the achievement of other common maneuvers, such as pitch/yaw rotation and linear swimming patterns. The proposed 2DOF soft swimming robot platform includes an underactuated, cable-driven design that mimics the flexible cascaded skeletal structure of soft spine tissue and hard spine bone seen in many fish species. The cable-driven actuation mechanism is oriented laterally for forwarding motion and steering in a 3D plane. The robot can perform a steady and controllable roll rotation with a maximum angular speed of 41.6 deg/s. A hypothesis explaining this novel roll rotation mechanism is set forth, and the phenomenon is systematically studied at different frequencies and phase lag gait conditions. Preliminary results show a linear relationship between roll angular velocity and frequency within a specific range. Additionally, the roll rotation can be controlled independently in some special conditions. These abilities form the foundation for future research on 3D underwater locomotion with adaptive, controllable maneuvering capabilities.

I. Introduction

Maneuverability, defined generally as the ability to change speed and direction, is one of the most important characteristics considered when studying the locomotion of natural, biological swimmers, and the design and evaluation of robotic swimmers. In nature, simple maneuvers include turning laterally (yaw) and dorsoventrally (pitch), rolling, starting, braking, and hovering [1], while more complex maneuvers can be generated from combinations of these. For example, whales can perform simple maneuvers (roll, yaw, and pitch change). At the same time, they can swim in a complex trajectory by combining these simple maneuvers sequentially (e.g., perform a banked turn by combining roll and pitch-up) [2]. In other words, a high maneuverability swimmer is necessary to, at least, be able to perform simple maneuvers (yaw, pitch, roll change). That is also the same truth for a swimming robot to achieve high maneuverability.

Among all the maneuvers, roll rotation is rare for fish but can be well performed by swimming mammals. Swimming mammals (e.g., sea otter, human) with flexible vertebra (able to bend in the transverse and vertical axis and twist along the longitudinal axis) can bend and twist their body in a waist-hooping-like motion to generate roll rotation.

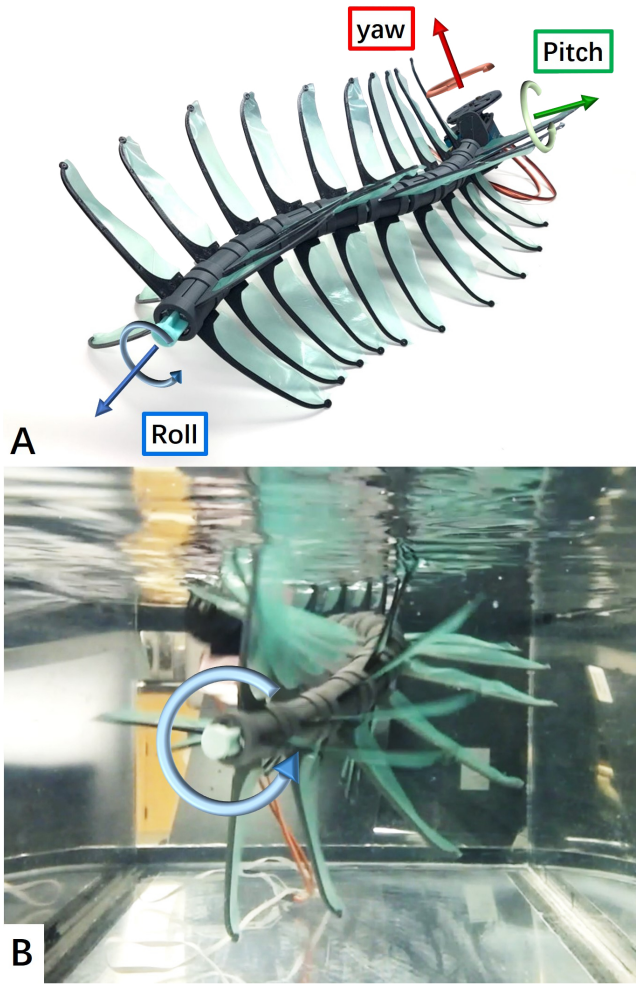

Fig. 1. The 2-DOF modular soft adaptive swimming robot: (a) The vertebrate-like modular robotic fish is made up of repetitive segments in series and actuated by two servos. (b) At a particular gait pattern, the robotic fish can swim in a helical shape and rotate roll angle.

Rotary and paddling propellers: To locomote underwater, many marine robots are mainly propelled by rotary propellers. Propellers are regarded as one of the more effective and reliable underwater propulsion mechanisms, which can either be powerful to propel the autonomous underwater vehicle (AUV) at high speed or control the position/orientation of a remotely operated vehicle (ROV) precisely [3]. Some other swimming robot using multiple

Bangyuan Liu and F. L. Hammond III are with the Woodruff School of Mechanical Engineering at the Georgia Institute of Technology, 313 Ferst Drive NW, Atlanta, GA 30332. bangyuanliu@gatech.edu, frank.hammond@me.gatech.edu

paddles to propel can also control 5 of its 6 DOF [4]. To achieve high maneuverability and controllability, it usually requires the robot to have multiple propellers.

Biomorphic oscillatory/undulatory swimming: Compared to conventional rotary propellers, many researchers believe biomorphic, fish-like swimming mechanisms would have benefits such as higher efficiency, higher maneuverability, and less noise [5][6][7]. However, as body roll rotation is an uncommon locomotion behavior for most types of fish, none of the previous fish-like swimming robots focused on the design of roll rotation mechanisms. [8][9].

Besides mimicking fish, other studies focused on mimicking a snake-like anguilliform (undulatory) swimming mode. These robots mimic undulatory swimming modes with fewer degrees of freedom (DOF), but are less maneuverable [10]. Some of them are multi-link servo robots, which have multi-DOF, leading to high maneuverability [11] [12].

Additional to the ability to achieve simple maneuver (roll, yaw, and pitch change), body flexibility is also another essential aspect that influences maneuverability. Several researchers have found that there is a general relationship between animal body flexibility and swimming maneuverability. Usually, the more flexible the body is, the higher maneuverability they would perform [1][2][13]. Some researchers designed the robots with a flexible body or flexible spine structure and studied their swimming performance[14][15], but none of them can achieve efficient roll rotation.

Roll rotation ability is undoubtedly necessary to perform a complex trajectory or swimming pattern to adapt to the complex underwater environment. It would be beneficial to discover/design an efficient roll rotation mechanism which lies between purely biomorphic and purely non-biomorphic. In other words, the swimming robot should have a more diverse function/swimming pattern than a biomorphic fish robot swimming mode, while being more flexible than non-biomorphic rotary propeller propelled AUVs.

In this paper, we discovered a novel biomorphic roll rotation mechanism by mimicking the swimming mammal's waist-hooping-like motion, which is based on our modular soft swimming robot (Fig. 1-A). The cost-effective swimming robot was improved from our previous work[16]. Besides the basic swimming mode ability (swim straight forward, rotate Pitch/Yaw angle), our two-DOF cable-driven robot can also achieve a steady and controllable roll rotation with a 41.6 deg/s maximum angular speed (Fig. 1-B). The roll rotation phenomenon is generated by two perpendicular sinusoidal body actuation wave with a specific phase lag. To better understand such a novel roll rotation mechanism, we also created a hypothesis that explains from the dynamic perspective. Moreover, we systematically studied the roll rotation phenomenon at different frequencies and phase lag conditions. From the preliminary test results, we found that the relationship between roll angular velocity and frequency is quite linear within a particular range. Besides, in some states, the robot can rotate roll angle while remains a relatively high forward velocity simultaneously. In some other states, it can rotate roll angle independently without forwarding locomotion. Such performance guarantees the robot with high maneuverability and controllability. And it would help later research on 3D space locomotion in the complex underwater environment.

II. Design of the 2DOF Swimming Robot

The flexible body is beneficial to design a swimming robot with high maneuverability, including biomorphic roll rotation capabilities. We improved our previous design to a 2DOF soft modular swimming robot[16]. The robot is cable-driven by two waterproofed servos. The body design is comprised of a bio-inspired vertebral-structure with certain flexibility created by soft joints. Besides, it is easy to assemble and disassemble to change components (adding/deleting vertebra, swap joints with different stiffness, and types of fins) for other future systematical tests. These components and their fabrication processes are described here.

A. Fabrication

The modular swimming robot is made up of multiple repetitive segments that mimic fish vertebral structures. Each single spine section consists of: hard 3D printed spine components which support the body structure; silicone joints which mimic intervertebral soft tissue and connect spine bone segments, forming bendable vertebra; and soft plastic membrane fins which provide additional propulsion force.

- **Cylindrical spine vertebrae**: The cylindrical spine vertebrae (h = 3.0 cm, d = 2.5 cm) are 3D printed (Stratasys uPrint SE Plus) in ABS material. These segments are comprised of two semi-cylinder parts and two rings (Fig. 2-C). The soft silicone joints and fins are press-fit onto two semi-cylinder parts and then stabilized by two circular rings (Fig. 2-C). The two semi-cylinders have small internal channels which the actuation wires pass through.
- **Soft elastic joints**: The soft elastic joints are cast from two types of silicone gel with different stiffness

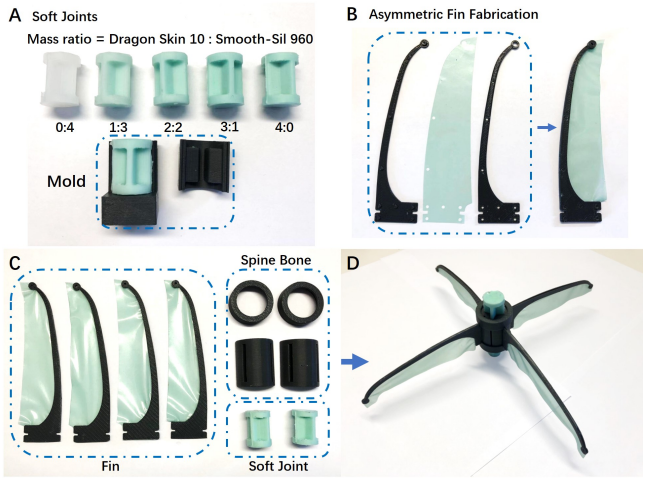

Fig. 2. Component Fabrication. (a) Molding of the soft joints with mixed silicone gel. The stiffness can be controlled by mixing ratio. (b) Assembling asymmetric fin. (c) Each segment consists of four fins, a pair of soft elastic joints, and cylindrical spine vertebrae. (d) A repetitive segment.

(Dragon skin 10 (Shore A Hardness: 10A) and Smooth-sil 960 (Shore A Hardness: 60A), Smooth-On, Inc.) in molds (h= 2.0 cm, d=1.5 cm). The 'X' cross-section shape enables itself to bend much more easily horizontally and vertically than in other directions, while still enabling the joint's ability to rotate in the roll direction. By changing the mixing ratio of two kinds of silicone gel, the joints' hardness can be controlled from 10A to 60A within the same shape. Fig. 2-A shows the mixed silicone joints with a mass mixing ratio from 0:4 to 4:0 (Dragon skin 10 : Smooth-sil 960).

- **Fins**: An asymmetric fin (Fig. 2-C left) is designed, which contains a flexible plastic sheet layer (Stretchlon 200 Bagging Film, Thickness: 0.381 mm) sandwiched by two 3D printed rigid fin frame parts (Fig. 2-B). It can produce strong propulsion in one certain direction when sweeping under the water.

Each repetitive segment is made up of a cylindrical spine vertebra with four fins and connected by soft joints (Fig. 2-D). The length of the modular soft swimming robot can be changed by the number of segments. Here we assembled a 38cm long swimming robot for the experiment (3.8cm×10) using ten segments. Two waterproofed servos (Savox SW1211SG) were attached on one side end of the body. Two sets of the Fishing line (d = 0.387 mm, load capacity = 18.5 kg) go through the small-sized tunnel within two sides of the cascaded spine bone segments, respectively, wrapping around and pulled by the wheels attached on each servo. One pair of servo-wire controls the bending of the yaw angle (Fig. 3-C) while another pair perpendicular to the previous pair controls the pitch angle (Fig. 3-D). When the two servos are positioned at the middle offset, the swimming robot is forced to align in a straight orientation (Fig. 3-A). When one of the servos rotates from the offset with a certain angle, one side of the corresponding wire is pulled on while another side wire is relieved, causing the whole cascaded spine structure to bend a specified amount (Fig. 3-B).

Each segment's buoyancy is close to the gravity, while the buoyancy of the servo is controlled by adding foam material to cancel out the influence of gravity.

III. Experiment Results and Discussion

In order to build a mapping between the swimming robot's actuation gait setting and its roll rotation performance, we studied how frequency and phase lag between two perpendicular sinusoidal body actuation waves (yaw and pitch) influence its roll angular velocity and linear velocity.

All of the experiments are carried out in a water tank (120 cm × 45 cm × 30 cm), and the modular soft swimming robot swims about the center to avoid the influence of boundaries.

A. Servo output characterization

The servos are controlled by periodically varying the duty cycle of a PWM (Pulse Width Modulation) signal generated by micro-controller (Arduino Nano) and powered by a 7.4 V lithium battery (1000 mAh, 20 C). By controlling the PWM signal command parameter f, the sweeping frequency can be controlled proportionally (Fig. 4-B). Compared to the previous paper, we improved the quality of servo (Savox SA1230SG changed by Savox SW1211SG)[16]. With a higher maximum angular velocity performance (previously: 0.16s/60 deg, currently: 0.08s/60 deg), the servo is able to generate a faster and steady rotation. The sweeping frequency shows a linear relationship versus input PWM signal command parameter f within the range of f=1-24. Besides, the sweeping range always remains the same as 180 deg. Correspondingly, all experiments are tested within a frequency range of 0.08 Hz-2.06 Hz.

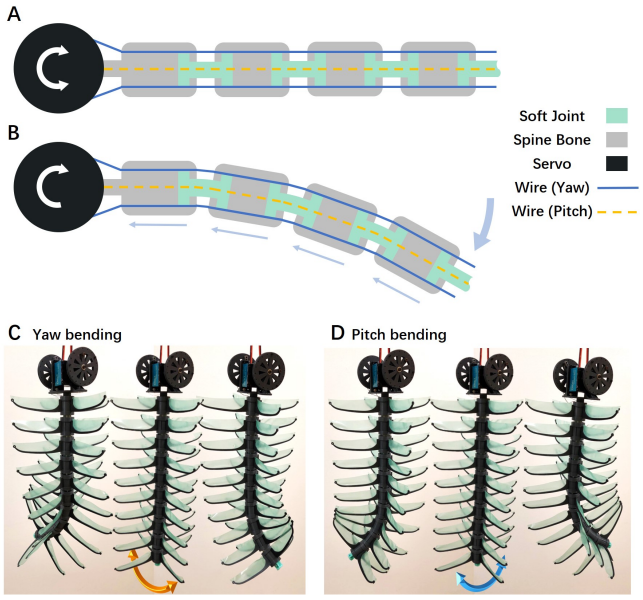

Fig. 3. An illustration of the swimming robot's actuation mechanism. The swimming robot is actuated by two pairs servo-wire and a sort of cable-driven lateral motion mechanism. When one servo rotates, one lateral wire is placed under tension, and while the opposite lateral wire is relaxed, forcing the elastic-beam-body structure to bend to one side. (c) and (d) shows the bending in yaw and pitch directions by actuating corresponding servos, respectively. By applying gait combinations, the swimming robot is able to propel and steer yaw, pitch, and even roll angle in different modes.

B. Roll rotation implementation

The roll rotation phenomenon is observed when the Yaw-servo and Pitch-servo (circled in blue and orange dash line in Fig. 5-A respectively) generates similar sinusoidal wave

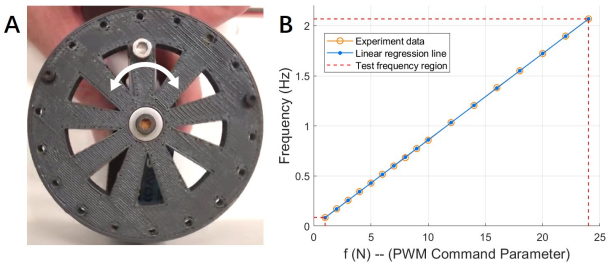

Fig. 4. Servo performance test. Servo rotation different frequencies without load is tested. (a) wheel attached to servo, whose motion is captured by a camera and analyzed. (b) real servo sweeping frequency versus the PWM signal command parameter f, mapping from f(1-24) to frequency (0.08 Hz-2.06 Hz) linearly. The servo's sweeping range always keeps at 180 deg.

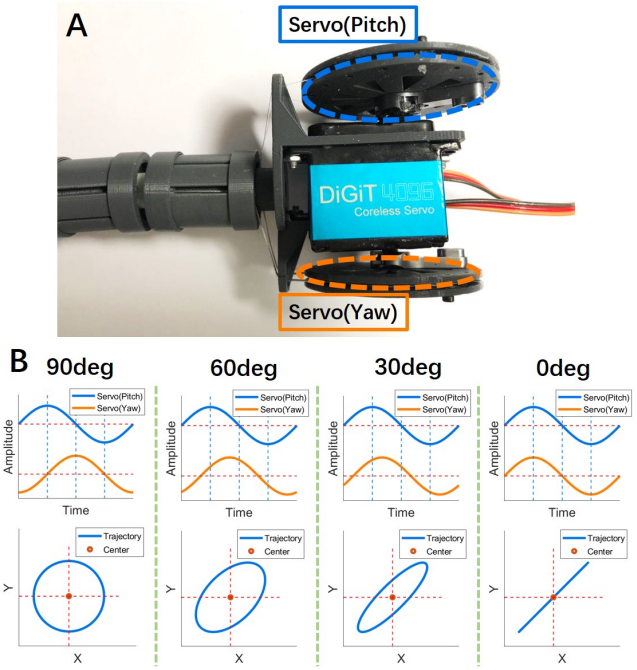

Fig. 5. Roll rotation implementation. (a) the robot is actuated by two servos (yaw and pitch). (b) by applying two sinusoidal actuation waves from the servos with a specific phase lag, the tail would create an elliptical trajectory. Here shows the waveform of two servos and the corresponding endpoint trajectory when a 90, 60, 30, 0 deg phase lag is applied, respectively.

sweeping output with a certain phase lag, as shown in Fig. 5-B with a 90, 60, 30, and 0 deg phase lag condition, respectively. The tail of the robot would move along an ellipse trajectory. (Especially, circle trajectory at 90deg phase lag, and linear trajectory at 0deg phase lag).

Fig. 6 shows the robot performance of roll rotation accompanied by forwarding swimming at 0.60 Hz frequency and 90deg phase lag condition. Screenshots were taken at 0s, 2s, 4s, and 6s. The robot rotates roll angle counter-clockwise with an averaged angular velocity of 41.6 deg/s. Simultaneously, the robot twists in a helical shape and swim forward at a velocity of 9.29 cm/s.

Additionally, the roll rotation direction can be controlled by changing the sign of phase lag. Fig. 7 shows the relationship between phase lag sign, body's helical trajectory direction (yellow dash circle with arrow), and body's roll rotation direction (red dash circle with arrow). When the phase lag is positive 90 deg (Fig. 7-A), the body's helical trajectory rotates counter-clockwise from an opposite perspective, while the body rotates roll angle clockwise. Correspondingly, when the phase lag is negative 90 deg (Fig. 7-B), the body's helical trajectory rotates clockwise while the body rotates roll angle counter-clockwise. For a short conclusion, the body's helical trajectory direction and body's roll rotation direction are always reverse to each other.

C. Roll Rotation Mechanism Hypothesis

According to the inverse relationship which we found between the body helical trajectory direction and body roll rotation direction, we made a hypothesis to explain such kind of novel roll rotation mechanism from the perspective of conservation of angular momentum. Here we use a two-segment simplified model to represent the robot's vertebra-mimicking body (Fig. 8-A). When the flexible body is actuated in a waist-hooping-like motion, the body motion consists of two rotation components. One is ω, which represents the roll rotation along the vertebra. Another is Ω, which represents the general rotation of the body center of mass. To maintain the conservation of angular momentum (as zero as started still), the ω and Ω would always reverse to each other in the Z-direction component in the world coordinate. However, when the vertebra body is not straight, and an angle θ exists between ω and Ω, the ω would be higher than Ω. As a result, the waist-hooping-like motion generates body roll rotation. Additionally, influenced by the hydrodynamic feature of fins, the pure waist-hooping-like roll rotation generates simultaneous forward swimming locomotion. Caused by the uneven mass distribution of the body (servo is much heavier than body segment), the head and tail do not rotate in the same phase. Consequently, the robot swims in a helical trajectory.

This hypothesis might be considered an "observation-to-conclusion" explanation, but there were two other viable hypotheses for this phenomenon: 1. The roll rotation is induced by the torque caused by non-collinear gravity and buoyancy, 2. The roll rotation is induced by the torque caused by the fins above water, which happens during some tests. To test these two hypotheses, we evaluated the robot's roll rotation ability in a water tank (7.0 m deep) by way of a vertical dive (Fig. 8-B). The robot still achieved roll rotation without any decrease in efficiency. As its body is in the vertical orientation and fully dived, there is neither sufficient non-collinear gravity and buoyancy torque to utilize for roll rotation, nor torque generated by the fins above water.

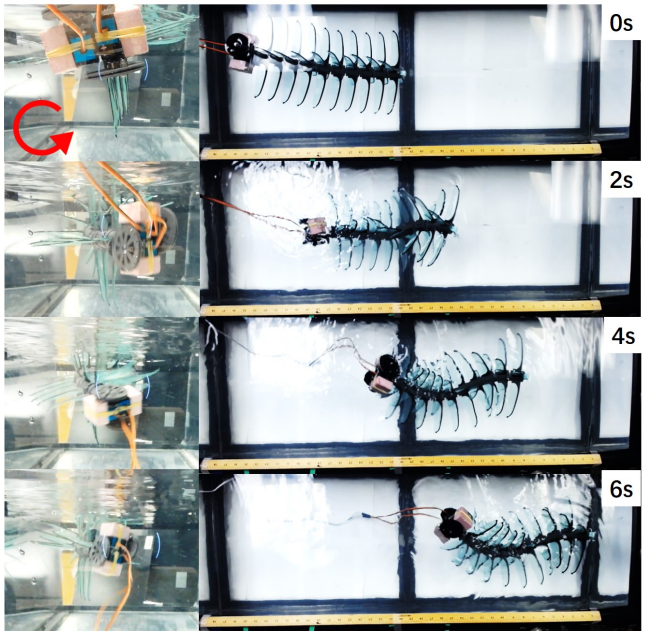

Fig. 6. The roll rotation swimming phenomenon at 0.60 Hz frequency and 90 deg phase lag condition. The roll rotation is also combined with forward swimming in certain conditions.

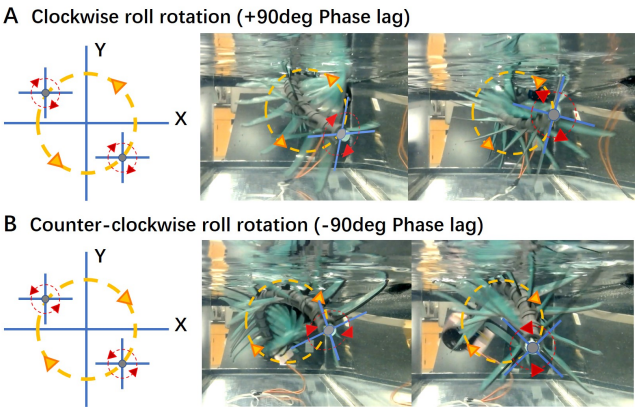

Fig. 7. A close view of the roll rotation phenomenon. (a) and (b) shows the kinematic schematic diagram and experiment result when applying a positive 90 and negative 90 phase lag. And the robot is able to rotate clockwise and counter-clockwise, respectively (form the opposite perspective). The frequency is 0.60 Hz.

Additionally, we believe other factors would also contribute to, or a more complex theory that would explain such kind of novel roll rotation mechanism. It is interesting to investigate further via experiment and simulation.

D. Impact of frequency and phase lag

As roll angular velocity and linear velocity are both functions of F(frequency, phase lag), this part of the experiment focused on mapping these relationships within a frequency range of 0.08 Hz-2.06 Hz and phase lag set of [90 deg, 60 deg, 30 deg, 0 deg] respectively. The distribution of spine joint stiffness has a positive gradient (stiffer close to the servo and softer further from the servo toward the tail) since this created more stable swimming patterns w.r.t. frequency changes in our previous study[16]. The fins are all set with a direction heading away from the servo. The swimming motions are captured by the camera. Roll angular velocity and linear velocity are analyzed in the video.

Fig. 9 shows the robot's roll rotation angular and linear velocities at different actuation frequencies and phase lags.

When focusing on the roll rotation angular velocity first (Fig. 9-A), generally, as frequency increases from 0.08 Hz, the angular velocity first increases linearly until it reaches the peak, which is enclosed by blue parallel dash lines (blue zone). Then the angular velocity decreases close to 0 when frequency continues increases to 2.06 Hz. These peaks are regarded as the swimming robot's roll rotation performance natural frequency. Regarding the impact of the phase lag, when the phase lag is higher than 60 deg (90 deg - blue curve, 60 deg - green curve), there is not any big angular velocity performance difference. It shows a linear decrease of the angular velocity when frequency increases after the natural frequency, enclosed by red parallel dash lines (red zone). However, when the phase lag continue decreasing to 30 deg (orange curve), while the roll angular velocity performance increasing region (blue zone) at a lower frequency remains the same, but the deceasing region (red zone) at higher frequency decreases. As soon as the phase lag is less than 15 degrees, the robot cannot rotate in the roll angle anymore (0 deg - purple curve). It seems that there is a small body potential well that needs enough roll rotation energy to conquer. Among all the phase lag conditions, 90 deg phase lag performs slightly better on roll rotation. At 90 deg phase lag and 0.60 Hz actuation frequency, the angular velocity reaches the maximum of 41.6 deg/s.

When focusing on the linear velocity (Fig. 9-B), as frequency increases, all results show the same trend that they first increase and then reach a plateau at high frequency. Limited by servo performance, we cannot carry on steady

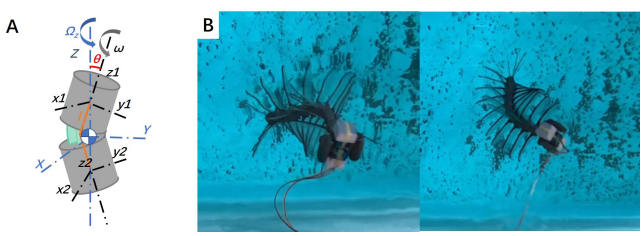

Fig. 8. Roll rotation mechanism hypothesis and verification. (a) shows the two rotation components ω and Ω when a simplified body model actuates in a waist-hooping-like motion during a roll rotation phenomenon. (b) shows the successful vertical roll rotation diving test in a 7.0 m deep water tank.

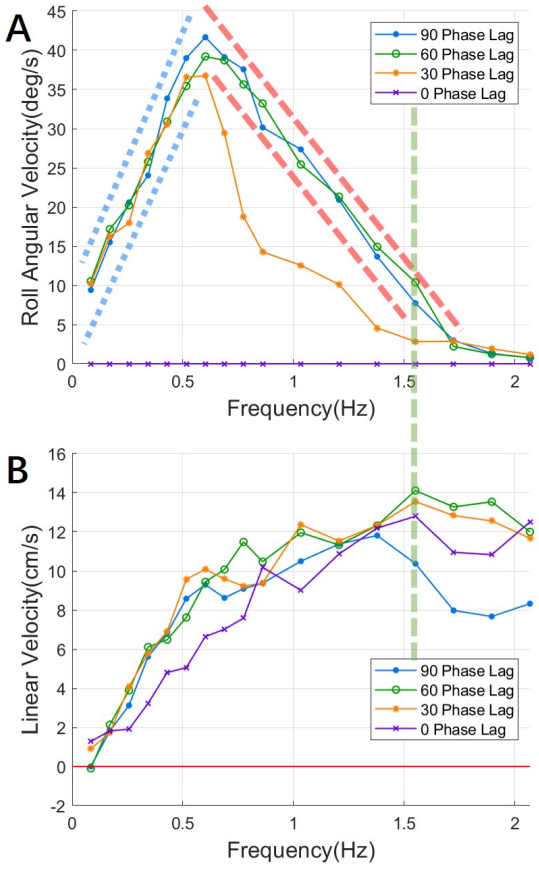

Fig. 9. The roll rotation swimming performance. (a) shows the impact of frequency and phase lag on roll angular velocity. The blue and red dash lines mark linear frequency regions. (b) shows the impact of frequency and phase lag on linear velocity. The area on the right side of the green line shows the frequency region that the linear velocity (with low angular velocity performance) at different phase lag diverges. The frequency range is 0.08-2.06 Hz. The four-color curves (1. blue, 2. green, 3. orange, 4. purple) represent the 90, 60, 30, 0 deg phase lag condition, respectively.

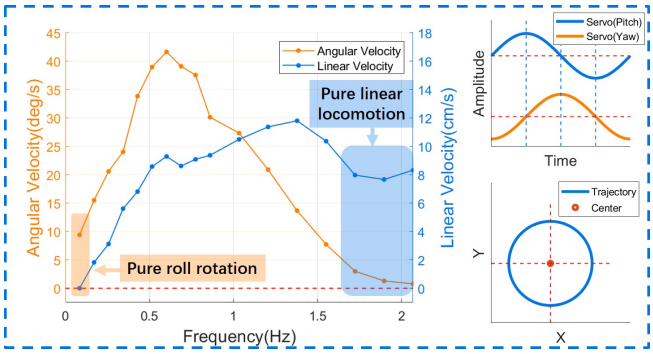

Fig. 10. The roll rotation performance at 90 deg phase lag condition. The orange area and blue area represents the conditions that only perform roll rotation and linear swimming, respectively.

tests at frequencies higher than 2.06 Hz. With different phase lag conditions, the linear velocity performance only shows a significant divergence at a frequency higher than 1.55 Hz. However, at such a high-frequency condition, the roll rotation will not perform well (the region on the right of the green dash line). That means within the efficient roll rotation frequency region (0.08 Hz-1.55 Hz), the linear velocity is not influenced by phase lag too much. Among all the phase lag conditions, 60deg phase lag performs slightly better on swimming forward while rotating roll angle. At 60 deg phase lag and 1.38 Hz actuation frequency, the linear velocity reaches the maximum, which is 14.11 cm/s.

E. Independent Roll Controllability

In addition to the performance discussed above, we find that the roll angle can be controlled independently. When focusing on a specific phase lag condition result (e.g., Fig. 10 shows the robot roll rotation angular velocity and Linear velocity results at 90 deg phase lag), the robot can rotate roll angle without apparent position locomotion at relatively low frequency due to the damping on the linear motion at low speed, shown in the orange region. At the same time, the robot can swim forward without apparent roll rotation, shown in the blue region. This consequence enables the robot to decouple roll rotation and forward swimming locomotion.

IV. Conclusion and Future Work

We discovered a novel roll rotation mechanism based on a simple modular soft swimming robot. The two-DOF cable-driven robot can achieve a steady and controllable roll rotation with a maximum angular speed of 41.6 deg/s in addition to the basic swimming mode ability (swim straight forward, rotate Pitch/Yaw angle). To explain such a roll rotation mechanism, we made a dynamical hypothesis and systematically studied the phenomenon at different gait conditions (different frequencies and phase lag). From the preliminary test, two important insights are gleaned. First, there is a particular linear region of the roll angular velocity and frequency relationship. Second, roll rotation can be performed independently. This performance and ability show the possibility of a 3D space swimming robot application with high maneuverability and controllability. With the slender flexible body, this roll rotation capability would help pass complex underwater obstacles, such as holes and tunnels.

Future work will include theoretical study and modeling of this roll rotation mechanism, test with different body configuration (body length, body stiffness distribution, fin configuration). To improve both the maneuverability and adaptability, we will also explore the design of soft stiffness-tunable joint mechanisms and deployable fins for real-time swimming mode transformation. Finally, an untethered version would be designed for later application.

Acknowledgment

The authors thank the George W. Woodruff School of Mechanical Engineering at Georgia Tech for the use of their Acoustic Water Tank facility, and Professor Daniel I. Goldman for providing access to his water tank testbed.

References

[1] J. A. Walker, "Does a rigid body limit maneuverability?" *Journal of Experimental Biology*, vol. 203, no. 22, pp. 3391–3396, 2000.

[2] P. Segre, D. Cade, J. Calambokidis, F. Fish, A. Friedlaender, J. Potvin, and J. Goldbogen, "Body flexibility enhances maneuverability in the worlds largest predator," *Integrative and comparative biology*, vol. 59, no. 1, pp. 48–60, 2019.

[3] S. Kang, J. Yu, J. Zhang, and Q. Jin, "Development of multibody marine robots: A review," *IEEE Access*, 2020.

[4] G. Dudek, P. Giguere, C. Prahacs, S. Saunderson, J. Sattar, L.-A. Torres-Mendez, M. Jenkin, A. German, A. Hogue, A. Ripsman *et al.*, "Aqua: An amphibious autonomous robot," *Computer*, vol. 40, no. 1, pp. 46–53, 2007.

[5] J. Liu, I. Dukes, and H. Hu, "Novel mechatronics design for a robotic fish," in *2005 IEEE/RSJ International Conference on Intelligent Robots and Systems*. IEEE, 2005, pp. 807–812.

[6] J. Yu and L. Wang, "Parameter optimization of simplified propulsive model for biomimetic robot fish," in *Proceedings of the 2005 IEEE International Conference on Robotics and Automation*. IEEE, 2005, pp. 3306–3311.

[7] J. Yu, M. Tan, S. Wang, and E. Chen, "Development of a biomimetic robotic fish and its control algorithm," *IEEE Transactions on Systems, Man, and Cybernetics, Part B (Cybernetics)*, vol. 34, no. 4, pp. 1798–1810, 2004.

[8] A. Phillips, "Robot fish: Bio-inspired fishlike underwater robots," *Underwater Technology*, vol. 34, no. 3, pp. 143–145, 2017.

[9] J. Zhu, C. White, D. Wainwright, V. Di Santo, G. Lauder, and H. Bart-Smith, "Tuna robotics: A high-frequency experimental platform exploring the performance space of swimming fishes," *Science Robotics*, vol. 4, no. 34, p. eaax4615, 2019.

[10] K. Struebig, B. Bayat, P. Eckert, A. Looijestijn, T. Lueth, and A. Ijspeert, "Design and development of the efficient anguilliform swimming robot-mar," *Bioinspiration & Biomimetics*, 2020.

[11] A. Crespi, A. Badertscher, A. Guignard, and A. J. Ijspeert, "Amphibot i: an amphibious snake-like robot," *Robotics and Autonomous Systems*, vol. 50, no. 4, pp. 163–175, 2005.

[12] S. Yu, S. Ma, B. Li, and Y. Wang, "An amphibious snake-like robot: Design and motion experiments on ground and in water," in *2009 International Conference on Information and Automation*. IEEE, 2009, pp. 500–505.

[13] J. M. Parson, F. E. Fish, and A. J. Nicastro, "Turning performance of batoids: limitations of a rigid body," *Journal of experimental marine biology and ecology*, vol. 402, no. 1-2, pp. 12–18, 2011.

[14] A. D. Marchese, C. D. Onal, and D. Rus, "Autonomous soft robotic fish capable of escape maneuvers using fluidic elastomer actuators," *Soft Robotics*, vol. 1, no. 1, pp. 75–87, 2014.

[15] Y. Zhong, Z. Li, and R. Du, "Robot fish with two-dof pectoral fins and a wire-driven caudal fin," *Advanced Robotics*, vol. 32, no. 1, pp. 25–36, 2018.

[16] B. Liu and F. L. Hammond, "Modular platform for the exploration of form-function relationships in soft swimming robots," in *2020 3rd IEEE International Conference on Soft Robotics (RoboSoft)*. IEEE, 2020, pp. 772–778.